

Simplified Method for the Identification of Low Mass Ratio Contact Binary Systems that are Potential Red Nova Progenitors

Surjit S. Wadhwa^{1*}, Ain Y. De Horta¹, Miroslav D. Filipović¹, Nick F. H. Tothill¹, Bojan Arbutina², Jelena Petrović³ and Gojko Djurašević³

¹School of Science, Western Sydney University, Locked Bag 1797, Penrith, NSW 2751, Australia.

²Department of Astronomy, Faculty of Mathematics, University of Belgrade, Studentski trg 16, 11000 Belgrade, Serbia.

³Astronomical Observatory, Volgina 7, 11060 Belgrade, Serbia

*Corresponding author. E-mail: 19899347@student.westernsydney.edu.au

Abstract. The study presents a simplified method to identify potential bright red nova progenitors based on the amplitude of the light curve and infrared (J-H) colour of a contact binary system. We employ published criteria for contact binary orbital instability to show that the amplitude of the light curve for a given contact system with a low mass ($< 1.4M_{\odot}$) primary must be less than a specified value for it to be potentially unstable. Using this we search the photometric data of a large survey to identify about 50 potential bright red nova progenitors. We analyse the survey photometry of each to determine the mass ratio and from the estimated mass of the primary other physical parameters of the systems. We show that each system has physical characteristics indicating potential orbital instability. Using the absolute parameters from our sample we model the expected instability separation and period for low mass contact binary systems.

Keywords. Contact Binary, Low Mass Ratio, light curve solution

1. Introduction

The number of known contact binary systems has, and still is, growing at a phenomenal rate given the new discoveries resulting from sky surveys. As an example, All Sky Automated Survey (ASAS) (Pojmanski, 2002) and the All Sky Automated Survey - Super Nova (ASAS-SN) (Shappee *et al.*, 2014; Jayasinghe *et al.*, 2020) have added more than 100000 new discoveries. Theoretical models such as Soker & Tyndala (2003); Eggleton (2012); Stępień (2011); Robertson & Eggleton (1977) predict that contact binary systems with extremely low mass ratios are likely to merge into a single rapidly rotating relatively cool giant star. The merger event is thought to result in a transient nova like event that evolves to remain bright in the red and infrared bands. The event is usually termed a red nova. Although Galactic merger events are predicted to occur commonly (once every 2-3 year), brighter events that are likely to be available for study are more limited at once a decade (Kochanek *et al.*, 2014). There has been only one confirmed observation linking typical red nova like transient to a contact binary progenitor, that of V1309 Sco (Tyndala *et al.*, 2011). Other examples such as V4432 Sgr (Martini *et al.*, 1999), V838 Mon (Brown *et al.*, 2002) and OGLE2002-BLG-360 (Tyndala *et al.*,

2013) are postulated to represent stellar mergers although their progenitors remain unidentified. In addition there exist possible historical and extra galactic examples (Pastorello *et al.*, 2019; Kochanek *et al.*, 2014). Since the recognition of V1309 Sco there has been heightened interest in the theoretical basis of orbital instability and the identification of low mass ratio contact binary systems (Wadhwa *et al.*, 2021; Gazeas *et al.*, 2021; Christopoulou *et al.*, 2022).

In two papers Rucinski (1993, 2001) showed that the shape of contact binary light curves is dependant on three main geometrical factors namely the mass ratio (q), the fill-out (f) (degree of contact - or the thickness of the contact neck region) and the inclination (i). In addition the other somewhat minor determinant is the temperature difference between the components. He deduced that the maximum amplitude for any given system was seen if the system was observed to have a complete eclipse. In addition, he showed that only the mass ratio, fill-out and to a lesser extent (in the presence of complete eclipses) inclination determined the amplitude of the light curve with other factors such as temperature of the components having little impact.

We combine the three techniques noted above namely the theoretical instability parameters, survey photometric data and the photometric amplitude distri-

bution of contact binary systems to derive a simplified method of identifying potential contact binary systems that show signs of orbital instability (potential red nova progenitors). For the purpose of this study we define a contact binary system with a mass ratio at or below the theoretical critical level as being potentially unstable. The paper is divided into five sections. In section two we model theoretical light curves to derive a relationship between the mass of the primary and the maximum amplitude of a potentially unstable system. In section 3 we employ the relationship to the ASAS-SN survey to identify potential bright red nova candidates among low mass ($0.6M_{\odot} < M_1 < 1.4M_{\odot}$) contact binary systems. In section 4 we define an average potential red nova progenitor in addition to comparing and contrasting our sample of bright potential red nova progenitors with other comparable systems. In section 5 we briefly discuss the historical development of mass ratio as a determinant of orbital instability, limitations of the present study and further ongoing search of red nova progenitors along with a summary and conclusion of the current work.

2. Amplitude Distribution of Potential Red Nova Progenitors

Critical to understanding the orbital evolution of contact binary system is predicated on knowledge of parameters such as the mass ratio, masses of the components and the geometry of the orbit such as inclination, degree of contact and temperature variation between the components. Many, if not all, of these parameters can be derived from light curve analysis but only if the light curve demonstrates a complete eclipse (Terrell & Wilson, 2005). As such, we limit our modelling of systems that demonstrate a complete eclipse and would be applicable to observed light curves

Current light curve analysis tools can incorporate many tens of different parameters, however, as noted above in the case of contact binary systems only 4 main parameters are critical. Therefore in modelling the amplitude distribution of unstable systems we have neglected complications associated with star spots and other stellar activity. We used the 2009 version of the Wilson-Devinney code as incorporated into the Windows front end utility WDwin56d (Nelson, 2021) to model all light curves. The gravity darkening coefficients $g_1 = g_2 = 0.32$, the bolometric albedos $A_1 = A_2 = 0.5$ were fixed (Lucy, 1967) and simple reflection treatment applied (Rucinski, 1969). As per Nelson & Robb (2015) logarithmic limb darkening coefficients interpolated from van Hamme (1993) were used.

To confirm the findings of Rucinski (1993, 2001)

with respect to the effects of fill-out and inclination on the amplitude of the light curve we modelled light curves of an idealised contact binary system with primary of one solar mass with mass ratio (q) 0.1 and equal temperature of the components ($T_1 = T_2 = 5770K$) to record the effects of inclination (i) and degree of contact ($f = 0 - 1$). As we are only interested in systems that display a total eclipse we modelled the system with an inclinations of 90° which would yield the maximum eclipse time and 72° which would yield a small total eclipse between phase 0.49 to 0.51. The change in inclination results in a reduction in the duration of the secondary eclipse with the lower inclination reducing the total amplitude slightly. We also modelled fill-out $f = 0$ and $f = 1$ for each inclination to determine the variation in amplitude and again to confirm previous findings using the current accepted modelling code. The fill-out has a significant effect on the amplitude of the light curve with high fill-out yielding the highest amplitude. This is as expected, because higher the degree of contact the thicker the neck of the contact region. The neck bears some luminosity and thicker the neck the greater the luminosity that is eclipsed. We did not model stars of different mass (hence different T_1) because as noted by Rucinski (2001) the combination chosen is a reasonable representation of the light curve of low mass contact binaries and confirms the previous findings that the maximum amplitude of a contact binary system occurs at high inclination and high degree of contact. The results are illustrated in Figure 1 and summarised in Table 1.

Having established the condition of high inclination and high fill-out for high amplitude we next modelled the effects of the difference in temperature of the components. The presence of a common envelope usually results in good thermal contact between the components so there is usually little difference in the temperatures of the components. Recently Latković *et al.* (2021) compiled a catalogue of published light curve solutions of contact binaries. Using a sub-sample of the catalogue for primary stars between ($0.6M_{\odot} < M_1 < 1.4M_{\odot}$) we determined the median temperature difference between the components of approximately 200K. Adopting the commonest temperature difference between the components we next modelled light curves for our idealised system with ($i = 90^\circ$ and $f = 1$) and temperatures of the secondary either 200K higher (5970K) or 200K lower (5570K). The results are illustrated in Figure 1 and summarised in Table 1. It is clear that the typical temperature difference has little effect on the maximum amplitude of the light curve with both the cooler or warmer secondaries having minimal impact relative to the result with the components being of same temperature. We can deduce from the above that

for any given mass ratio the maximum amplitude will be achieved with high inclination, high fill-out and the secondary slightly warmer.

Inclination(°)	fill-out	T_2	Max Ampl (Mag)
90	1	Eq	0.36
72	1	Eq	0.31
90	0	Eq	0.27
90	1	CS	0.36
90	1	HS	0.36

Table 1. Effects of inclination, fillout and temperature of the secondary on the maximum amplitude of a contact binary system with mass ratio 0.1. Eq = Equal component temperatures, CS = Cold Secondary, HS = Hot secondary, $r_{1,2}$ = mean fractional radii of primary and secondary.

Having establish the modelling criteria for the maximum amplitude at a given mass ratio we employ this to determine the maximum amplitude of a potential red nova progenitor. Recently Wadhwa *et al.* (2021) linked the instability mass ratio of contact binary systems with the mass of the primary component. They demonstrated that the mass ratio at which instability (q_{inst}) is likely can be determined by a simple quadratic relationship for high and low level of contact:

$$q_{inst} = 0.1269M_1^2 - 0.4496M_1 + 0.4403 \quad (f = 1). \quad (1)$$

$$q_{inst} = 0.0772M_1^2 - 0.3003M_1 + 0.3237 \quad (f = 0). \quad (2)$$

Using this relationship say for a system with primary of one solar mass the instability mass ratio at high fill-out would be approximately 0.12. If we now model a light curve with the following parameters $T_1 = 5770K$, $T_2 = 5970K$, $i = 90^\circ$, $f = 1$ and $q = 0.12$ this will give us the maximum amplitude at which such a system is possibly unstable. As amplitude increases with increasing mass ratio (see below and Rucinski (1993, 2001)), any system with amplitude higher will likely have a higher mass ratio and therefore would be stable. As inclination of a system drops eventually a complete eclipse is lost and light from both components is observed throughout the orbital cycle and the overall variation (amplitude) of the light curve drops (Rucinski, 2001). Therefore a system with amplitude significantly below the maximum amplitude is unlikely to have a complete eclipse and therefore not suitable for photometric light curve analysis. We extended our modelling of the maximum amplitude for systems with primary star masses between $0.6M_\odot$ and $1.4M_\odot$ and the calculated instability mass ratio at high fill-out. We adopted values of T_1 based on the main sequence calibration

from (Pecaut & Mamajek, 2013) + 200K. The results are summarised in Table 2 and the line of best fit is as shown in Eq 3 and graphically shown in Figure 2. It is clear that higher the mass ratio the greater the amplitude therefore any system with an amplitude higher than that predicated at the theoretical instability mass ratio will likely have a mass ratio above the instability value and therefore be likely stable.

Mass (M_1)(M_\odot)	$q_{inst}(f = 1)$	Max Ampl
0.6	0.22	0.63
0.7	0.19	0.60
0.8	0.16	0.52
0.9	0.14	0.45
1.0	0.12	0.43
1.2	0.08	0.32
1.4	0.06	0.22

Table 2. Summary of the maximum amplitude at the instability mass ratio (q_{inst}) for systems with low mass primary component.

$$MaxAmpl(mag) = -0.5179M_1 + 0.945 \quad (3)$$

3. Search for Potential Red Nova Progenitors

As noted above we confined our search to bright systems with lower mass ($0.6M_\odot < M_1 < 1.4M_\odot$) primaries. The ASAS-SN variable database provides a friendly user interface to select variable stars of different types. We used this to select all contact binaries brighter than 13.5 magnitude. We limited our search to brighter examples as random review of the ASAS-SN light curves indicated that fainter examples had too much scatter and in most cases it was impossible to visually confirm the presence of complete eclipses and/or the amplitude of the light curve. A secondary benefit for favouring brighter examples is the potential ease in obtaining long term follow up monitoring. The selected systems are within the reach of modest instruments and could potentially be observed regularly by campus based telescopes or even by advanced amateurs. The systems were then ordered by amplitude and all systems with amplitude greater than 0.65 were excluded as the maximum amplitude for a $0.6M_\odot$ primary with a mass ratio at the instability level ($q_{inst} = 0.22$) is 0.63 magnitudes.

It is well established that the primary component of a contact binary systems follows in general a main sequence profile (Yildiz & Doğan, 2013). The ASAS-SN database also provided the J and H magnitude for

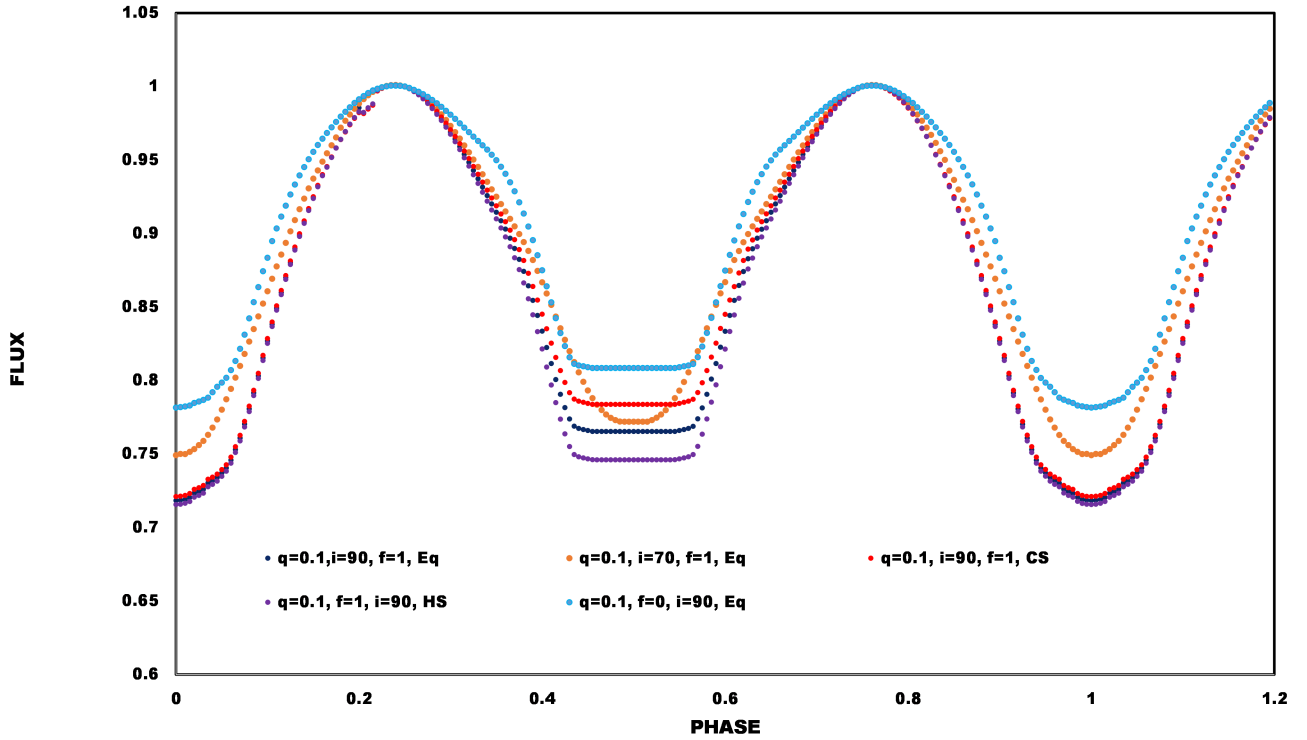


Figure 1. Effects of inclination, fillout and temperature of the secondary on the maximum amplitude of a contact binary system with mass ratio 0.1. Eq = Equal component temperatures, CS = cooler secondary, HS = hotter secondary.

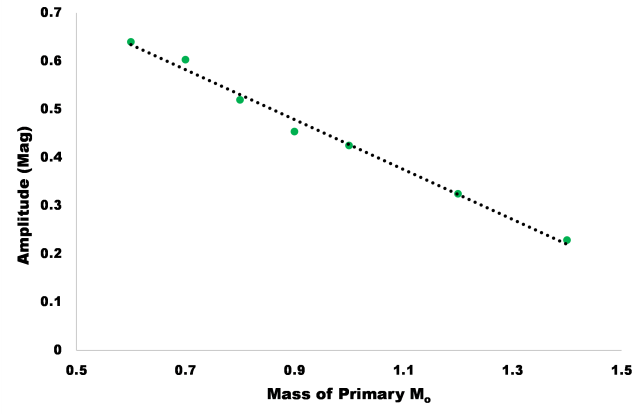


Figure 2. Maximum amplitude of contact binary systems with mass of the primary between $0.6M_{\odot}$ and $1.4M_{\odot}$ and mass ratio at the instability level ($f=1$).

each system. We calculated the J-H magnitude for each system and using the calibration for low mass (F3-K9) main sequence stars of Pecaut & Mamajek (2013) we interpolated the mass and effective temperature of the primaries. All systems with masses outside our inclusion criteria were excluded. The remaining systems

were examined visually to determine the presence of a total eclipse. Only those systems where a clear total eclipse were included. We note that such a crude selection system is likely to include or exclude some systems in the final sample. A more robust system of checking the variability within a defined time interval of the eclipses proved unworkable due to the cadence and scatter in many systems. The final sample totaled 189 contact binary systems. Having established the mass of the primaries for our selected 189 samples we next determined the instability mass ratio for each using Eq 1 and the maximum amplitude using Eq 3. We next compared the amplitude of the survey light curve against the maximum amplitude for potential instability. If the observed amplitude was significantly ($> 5\%$) higher than the maximum instability amplitude than such a system would be expected to have a mass ratio higher than the instability mass ratio and not be considered a potential merger candidate. All systems identified as such were excluded. The 5% leeway is arbitrary to account for the scatter normally present in survey data. This step left a sample of 65 systems of potential red nova progenitors.

Even though the ASAS-SN light curves were of reasonable quality we searched the VSX database as

well as the TESS and Kepler variable databases for all available light curves for the 65 systems. All light curves found from other databases were compared with the available ASAS-SN light curves and if they offered better phase coverage and clearer eclipses they were chosen for the formal light curve analysis instead of the ASAS-SN curves. Although where TESS data was available it provided the cleanest curves we did in some cases use the ASAS-SN, Catalina survey (Drake *et al.*, 2017) and SWASP Survey (Pollacco *et al.*, 2006) photometry.

All the selected light curves from the final sample were analysed using the Wilson-Devenney code as noted above. We used the standard mass ratio search grid method to find the probable mass ratio for each system. Temperature of the primary was fixed according to the main sequence calibration of Pecaut & Mamajek (2013). Logarithmic limb darkening coefficients were interpolated from van Hamme (1993). The TESS and Kepler photometric data is provided as a flux and this was converted to magnitudes using the calibrations from Handberg *et al.* (2021) and Aigrain *et al.* (2015) respectively. We used the MIT Quick Look pipeline for the optimal aperture for the TESS data (Huang *et al.*, 2020) and K-2 data when using Kepler mission data. The TESS photometry was acquired over a broad red to infra-red window centered on the standard I_c band (786.5nm) (Ricker *et al.*, 2015). We used limb darkening coefficients for the I_c band when analysing the TESS data. The Kepler and SWASP photometry was acquired with wide-band filters from blue to red (Van Cleve *et al.*, 2010; Pollacco *et al.*, 2006) and we used limb darkening coefficients for the central V band.

Given the scatter and potential incomplete phase coverage some of the systems upon analysis had a mass ratio above the instability mass ratio suggesting that the amplitude is probably higher than that measured by survey photometry. As noted by Christopoulou *et al.* (2022) a small uncertainty in the mass of the primary can result in a modest uncertainty in the instability mass ratio. Accordingly, for the purpose of this study we consider any system with a mass ratio below or up to 10% above the theoretical maximum instability mass ratio to be potentially a red nova candidate. From our initial sample of 65 there were 45 that met the instability criteria and the basic parameters of these are summarised in Table 3. Abbreviation and cross matching of individual systems are presented in Table 5. The list will of course in the future be refined as the mass of the primary of these systems is more accurately determined. It must be stressed that this study only covers the ASAS-SN variable database. Given the sheer number of bright contact binaries (magnitude ≤ 13.5) listed on the VSX (≈ 20000) at this time we have not

systematically reviewed other survey data (some with poor search interfaces) for more examples. We hope to do this over time and add to the list progressively. For completeness we do add some examples to the list from the existing literature as described below.

4. Absolute Parameters and the Average Potential Red Nova Progenitor

4.1 Absolute Parameters

We determined the absolute parameters for each system from the light curve solution and period of the system. As noted above mass of the primary was estimated from the J-H colour of each system. The mass ratio provides the mass of the secondary. The relative radii of the components are dependant on the mass ratio and Roche geometry as by definition both components overflow their inner Roche lobes in a contact binary system. The light curve solution provides fractional radii of the components ($a_{1,2}, b_{1,2}, c_{1,2}$) in three orientations. The geometric mean of these was used to estimate $r_{1,2} = \sqrt[3]{a_{1,2}b_{1,2}c_{1,2}}$. The separation (A) between the components was determined using Kepler's third law and the absolute radii of the components were determined as per (Awadalla & Hanna, 2005) $R_{1,2} = A \times r_{1,2}$.

By way of comparison with other contact binary systems we looked at our list of possible red nova progenitors with low mass ($0.6M_{\odot} < M_1 < 1.4M_{\odot}$) primary contact binary systems listed by Latković *et al.* (2021). We accepted as true the masses determined by the publishing authors regardless of the methodology employed. Allowing for a 10% margin the final list of 300 systems includes 9 systems that would be classified as potential red novas progenitors based on the instability criteria outlined above. Of these 9, three were already included in our list while the others were either fainter than our cut-off limit, had poor phase coverage and in two cases were too bright for the ASAS-SN survey equipment. We have added these to our final list of potential red nova progenitors relying on the published absolute parameters. As the catalogue of Latković *et al.* (2021) covers literature to the early part of 2021 we performed a literature search from March 2021 to March 2022 for any new reported contact binary systems that may be regarded as red nova progenitors. This resulted in the addition three more potential systems. In total we catalogue 54 low mass ratio contact binary systems that maybe regarded as potential red nova progenitors (Table 3).

The period distribution of low mass contact binary systems ($0.6M_{\odot} < M_1 < 1.4M_{\odot}$) as adopted from Latković *et al.* (2021) as a whole relative to potential

Name	Period	q	q_{inst} range	T_1	T_2	$M_1(M_\odot)$	$R_1(R_\odot)$	$R_1/ZAMS$	Survey	References
A0006	0.38318	0.115	0.108 - 0.128	5700	5699	0.95	1.34	1.39	TESS	
LM Psc	0.34013	0.096	0.082 - 0.094	6075	6241	1.13	1.33	1.19	ASAS-SN	
A0346	0.30717	0.148	0.139 - 0.171	5120	5043	0.77	1.05	1.29	TESS	
A0458	0.33348	0.086	0.082 - 0.093	6100	5625	1.14	1.3	1.16	TESS	
A0514	0.34572	0.127	0.116 - 0.138	5600	5626	0.9	1.22	1.32	TESS	
NSVS 470	0.35576	0.078	0.095 - 0.110	5900	6231	1.04	1.37	1.32	TESS	
V644 Pup	0.33056	0.14	0.132 - 0.161	5300	5824	0.8	1.12	1.33	TESS	
A0842	0.33353	0.1	0.086 - 0.098	6040	6315	1.1	1.3	1.23	TESS	
A1037	0.34370	0.09	0.070 - 0.085	6200	6081	1.21	1.34	1.14	CATALINA	
A1214	0.39850	0.085	0.099 - 0.116	5850	5786	1.01	1.43	1.41	KEPLER	
A1249	0.37191	0.095	0.091 - 0.104	5950	5948	1.07	1.39	1.3	TESS	
A1251	1.05207	0.085	0.073 - 0.082	6200	5599	1.21	2.89	2.45	TESS	
SSS1315	0.38281	0.075	0.108 - 0.128	5700	5330	0.95	1.39	1.44	CATALINA	
A1407	0.36358	0.088	0.086 - 0.098	6040	6105	1.1	1.39	1.27	TESS	
A1446	0.35170	0.09	0.116 - 0.138	5600	5369	0.9	1.28	1.39	TESS	
A1517	0.32518	0.1	0.132 - 0.161	5300	5368	0.8	1.13	1.34	ASAS-SN	
A1531	0.83309	0.085	0.082 - 0.093	6100	5812	1.14	2.43	2.17	KEPLER	
V396 Lup	0.36324	0.132	0.120 - 0.145	5500	5794	0.88	1.27	1.39	TESS	
A1629	0.31077	0.059	0.104 - 0.122	5800	6115	0.98	1.22	1.23	ASAS	
A1651	0.35321	0.152	0.129 - 0.157	5300	5158	0.82	1.19	1.38	TESS	
V565Dra	0.39032	0.092	0.091 - 0.104	5970	6055	1.07	1.42	1.34	TESS	
A1751	0.93521	0.105	0.095 - 0.110	5900	5551	1.04	2.46	1.49	ASAS	
A1846	0.30284	0.162	0.130 - 0.160	5250	5148	0.8	1.06	1.25	KEPLER	
A1847	0.68961	0.077	0.077 - 0.087	6150	5917	1.18	2.18	1.89	ASAS-SN	
A1907	0.76308	0.06	0.093 - 0.106	5970	5619	1.07	2.32	2.18	ASAS-SN	
A1928	0.32002	0.08	0.082 - 0.093	6100	6120	1.14	1.26	1.13	SWASP	
A1946	0.38378	0.1	0.120 - 0.144	5520	5524	0.88	1.3	1.43	ASAS-SN	
A2001	0.35088	0.12	0.123 - 0.140	5450	5614	0.86	1.18	1.33	ASAS-SN	
A2003	0.45720	0.127	0.107 - 0.128	5720	5613	0.95	1.52	1.58	ASAS	
A2044	0.34289	0.103	0.099 - 0.116	5800	5751	1	1.29	1.28	TESS	
A2044	0.37054	0.07	0.082 - 0.093	6100	6076	1.14	1.45	1.29	ASAS-SN	
NSVS 114	0.35470	0.096	0.116 - 0.138	5580	5572	0.9	1.28	1.38	ASAS-SN	
A2048	0.80583	0.115	0.104 - 0.122	5800	5870	0.98	2.2	2.23	SWASP	
A2132	0.31634	0.1	0.108 - 0.127	5700	5953	0.95	1.18	1.22	TESS	
A2145	0.35385	0.075	0.099 - 0.116	5850	5770	1.01	1.32	1.3	TESS	
SSS 2213	0.36990	0.08	0.082 - 0.093	6100	6249	1.14	1.42	1.26	TESS	
A2222	0.40609	0.133	0.116 - 0.138	5580	5853	0.9	1.38	1.49	TESS	
A2243	0.33535	0.085	0.091 - 0.104	6000	6004	1.07	1.29	1.22	TESS	
A2250	0.31196	0.132	0.126 - 0.153	5400	5584	0.84	1.11	1.26	SWASP	
A2258-26	0.32764	0.093	0.084 - 0.095	6050	5955	1.12	1.29	1.17	SWASP	
A2258	0.30946	0.162	0.129 - 0.157	5300	5496	0.82	1.05	1.22	ASAS-SN	
NSVS 902	0.32510	0.108	0.104 - 0.122	5800	5718	0.98	1.19	1.21	SWASP	
A2348	0.34719	0.108	0.091 - 0.104	5970	5807	1.07	1.29	1.22	SWASP	
V1222 Tau	0.29536	0.104	0.116 - 0.138	5600	5439	0.9	1.06	1.15	LIT	Liu <i>et al.</i> (2015)
NSVS 431	0.25596	0.147	0.151 - 0.188	6000	5875	0.7	0.87	1.14	LIT	Kjurkchieva <i>et al.</i> (2020)
A0822	0.28005	0.11	0.087 - 0.099	5960	6080	1.1	1.1	1.01	LIT	Kandulapati <i>et al.</i> (2015)
GSC 0341	0.27716	0.055	0.092 - 0.106	5870	5828	1.06	1.17	1.1	LIT	Li <i>et al.</i> (2021)
A0832	0.31132	0.067	0.072 - 0.081	6300	6602	1.22	1.34	1.13	LIT	Sriram <i>et al.</i> (2016)
NSVS 780	0.28120	0.098	0.141 - 0.173	5490	5706	0.79	1.1	1.31	LIT	Popov <i>et al.</i> (2021)
PZ UMA	0.26267	0.178	0.139 - 0.170	5430	4972	0.77	0.92	1.12	LIT	Zhou & Soonthornthum (2019)
NSVS 256	0.28780	0.078	0.078 - 0.088	6030	6100	1.17	1.19	1.04	LIT	Kjurkchieva <i>et al.</i> (2018)
SX Crv	0.31662	0.079	0.069 - 0.077	6340	6160	1.25	1.32	1.09	LIT	Zola <i>et al.</i> (2004)
A1328	0.38470	0.086	0.071 - 0.079	6300	6319	1.23	1.49	1.25	LIT	Li <i>et al.</i> (2021)
ZZ PsA	0.37389	0.078	0.086 - 0.098	6514	6703	1.213	1.42	1.24	LIT	Wadhwa <i>et al.</i> (2021)

Table 3. Summary of the pertinent light curve solution and absolute parameters of potential red nova progenitors. Entries marked with "LIT" have been taken from the literature. They were not identified from examination of the ASAS-SN light curves as described. q_{inst} range is the instability mass ratio from $f = 0 - 1$.

red nova progenitors is illustrated in Figure 3. The median period for the entire sample is in the order of 0.330 days, only marginally less than 0.346 days for potential red nova progenitors. Most of the systems in both groups have periods between 0.25 and 0.5 days although the peak in the distribution around 0.35 days is more pronounced in the potential red nova progenitor sample. There is a hint of possibly some systems with higher periods being more common in the potential red nova progenitors group. The finding is in line with Kobulnicky *et al.* (2022) who found that extreme mass ratio systems tended to have a slightly increased frequency of longer periods.

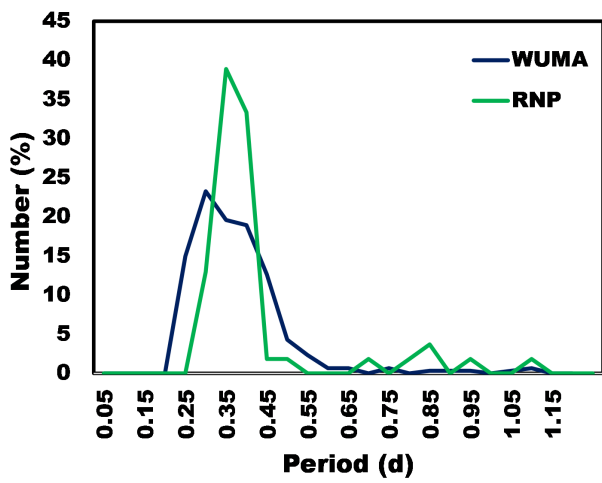


Figure 3. The period distribution of Red Nova Progenitors (RNP) relative to population of low mass contact binary systems (WUMA). Systems binned over 0.05 days

4.2 Average Potential Red Nova Progenitor

Based on the work of Arbutina (2007), Wadhwa *et al.* (2021) the separation at the onset of instability (A_{inst}) can be written as:

$$\frac{A_{inst}}{R_1} = \frac{q \frac{k_2^2}{k_1^2} PQ}{q \frac{k_2^2}{k_1^2} P^2 + \frac{q}{(1+q)k_1^2}} + \frac{\sqrt{(q \frac{k_2^2}{k_1^2} PQ)^2 + 3(1 + q \frac{k_2^2}{k_1^2} Q^2)(q \frac{k_2^2}{k_1^2} P^2 + \frac{q}{(1+q)k_1^2})}}{q \frac{k_2^2}{k_1^2} P^2 + \frac{q}{(1+q)k_1^2}} \quad (4)$$

where $k_{1,2}$ is the gyration radius for the primary and secondary components and

$$P = \frac{0.49q^{2/3} - 3.26667q^{-2/3}(0.27q - 0.12q^{4/3})}{0.6q^{2/3} + \ln(1 + q^{1/3})}, \quad (5)$$

$$Q = \frac{(0.27q - 0.12q^{4/3})(0.6q^{-2/3} + \ln(1 + q^{-1/3}))}{0.15(0.6q^{2/3} + \ln(1 + q^{1/3}))}. \quad (6)$$

Assuming our sample of potential red nova progenitors as representative we find the median radius ($\pm SD$) of the primary to be 1.285 (± 0.3) times the corresponding ZAMS equivalent. As noted previously the primary of contact binary systems can be considered as ZAMS so we can estimate the typical radius and hence the instability separation for a typical potential red nova progenitor. We perform this for low mass contact binary systems with low and high degree of contact as described in Wadhwa *et al.* (2021) and adopt the mean. Using equations outlined above and mean instability separation we estimate the mean period at the onset of instability (P_{inst}) for low mass contact binary systems. The results are summarised in Table 4. From these we derive simple quadratic relations (Figures 4 and 5) linking the mass of the primary with the instability separation and period as follows:

Mass (M_1)(M_\odot)	$A_{inst}(M_\odot)$	$P_{inst}(d)$
0.6	1.571	0.269
0.7	1.738	0.293
0.8	1.899	0.316
0.9	2.054	0.339
1.0	2.202	0.359
1.1	2.339	0.378
1.2	2.459	0.393
1.3	2.556	0.402
1.4	2.620	0.403

Table 4. Separation and Period at the onset of instability for modelled potential red nova progenitors

$$A_{inst} = -0.6766M_1^2 + 2.6932M_1 + 0.1878 \quad (7)$$

$$P_{inst}(d) = -0.1446M_1^2 + 0.4645M_1 + 0.0401 \quad (8)$$

From the above we see that a typical one solar mass contact binary system that is near the onset of instability will have a mass ratio near 0.12, maximum light curve amplitude near 0.43 and period near 0.36d. As a means of selecting potential low mass ratio contact binary stars for photometric analysis one could follow the relationships described to select candidates that are more likely to reflect features of orbital instability.

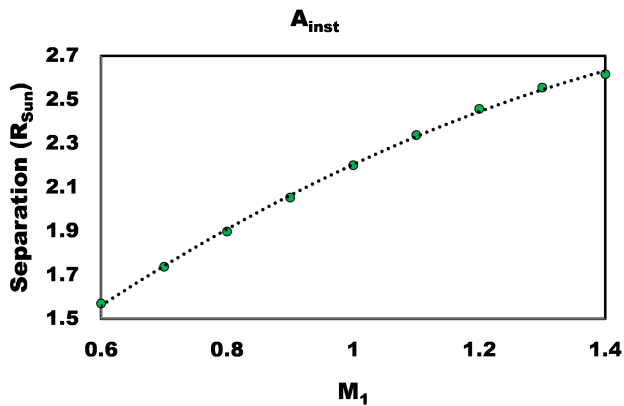


Figure 4. Instability separation for low mass contact binary systems.

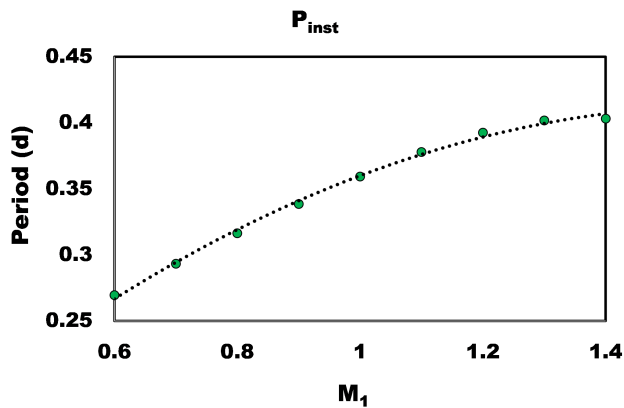


Figure 5. Instability period for low mass contact binary systems.

Given the inherent scatter and varying cadence of survey photometry we stress the above analysis is only an aid in the selection process and follow up observations would be required to confirm instability criteria that maybe evident on survey photometry. We are however confident given the success of survey photometric analysis compared to dedicated ground based observations in determination of accurate light curve solutions (Sun *et al.*, 2020; Devarapalli *et al.*, 2020; Wadhwa *et al.*, 2022) that if the survey data is chosen to ensure high cadence, low scatter and full phase coverage than the properties deduced from such data would be confirmed on follow-up study and hence are confident that the systems selected represent potential red nova progenitors.

5. Discussion and Conclusions

Although contact binary merger events are predicted to be relatively frequent so far only a single event has

been confirmed and that only in retrospect. The linking of orbital stability with the mass ratio of contact binary systems has long been recognised as potential avenue for identifying unstable systems (Rasio, 1995; Arbutina, 2007, 2009). The earlier work clearly showed that orbital instability is likely to occur at very low mass ratios and higher mass ratio configurations are likely to be stable. Our theoretical work (Wadhwa *et al.*, 2021) linking the instability mass ratio to the mass of the primary has progressed this further by demonstrating that there exists no global minimum mass ratio at which a system will become unstable rather the instability mass ratio is dependant on the mass of the primary component. In addition, we showed that systems with less massive primaries can have mass ratios higher than 0.2 and still be potentially unstable. When combined with work showing the suitability of survey photometry for light curve analysis (Sun *et al.*, 2020; Devarapalli *et al.*, 2020; Wadhwa *et al.*, 2022) has greatly facilitated the potential for being able to identify low mass ratio contact binary systems. In this study we enhance this capability by establishing simple light curve and colour parameters that can be used to exclude systems that are likely to have mass ratios above the theoretical instability value. By excluding likely stable systems we greatly increase our chance of identifying potentially unstable systems from the remaining sample. We apply the techniques on bright contact binary systems from the ASAS-SN and identify approximately 50 extreme low mass ratio system (most previously not reported) satisfying the mass ratio criteria for orbital instability.

As with almost all low mass contact binary systems (Latković *et al.*, 2021) our identified sample of potential merger candidates demonstrate radii that are significantly larger than their main sequence counterparts and secondaries that are considerably hotter than main sequence counterparts of similar mass. We find that relative to the general population of comparable contact binaries those exhibiting signs of orbital instability generally have similar periods although with a more pronounced peak near 0.35d. In addition there is a significant number of systems, relative to the general population, that have longer ($> 0.5d$) periods. Kobulnicky *et al.* (2022) suggest that it is possible for the period to lengthen to above 0.5d in some cases of extreme low mass ratios and the onset of orbital instability. In this respect our sample of possible unstable systems with long periods represent a good subset study group for future observations.

From our sample of potential red nova progenitors we construct theoretical models for low mass potentially unstable contact binary systems which place further constraints on the light curve morphology and timings. We note that for low mass systems there is a

narrow period domain from $\approx 0.27d$ to $0.4d$ at which they may become unstable and this increases with the mass of the primary. Those results will further aid in the identification of potential red nova progenitors from large survey samples. We hope to employ all the techniques and modifications described to the VSX database to further identify bright potential red nova candidates.

The techniques described in no way ensure all potential red nova progenitors are identified. Limiting our selection to those exhibiting complete eclipses clearly excludes a significant portion of contact binary systems, however, identification of potential systems among these would require both time consuming dedicated observations on modest sized telescopes and high resolution spectroscopic observations. Such requirements are unlikely to be readily available. The light curves of non totally eclipsing systems cannot be reliably analysed due to the high degree of correlation between the three geometric parameters specifically the inclination, mass ratio and degree of contact. The presence of a total eclipse places significant constraints, particularly in the q/i , domain allowing for manual search to be performed to find the correct light curve solution. Also, as already noted, survey photometric data although useful in light curve analysis does have limitations given the scatter, particularly with respect to the determining the fill-out fraction (Devarapalli *et al.*, 2020; Wadhwa *et al.*, 2022). Looking at Equations 1 and 2 above we see that the fill-out can have a significant influence on the instability mass ratio particularly for systems with the primary below one solar mass. The methodology employed places sorting restrictions assuming a high fill-out so it is possible that some of the identified samples may still be in the stable range. The small sample identified offers a good opportunity for dedicated observations with modest optical instruments to further refine the list of potential merger candidates. To this end we have started a programme of dedicated multi-band observations of some of the identified systems with instruments in the 0.5m range with results to be presented progressively.

Acknowledgements

Based on data acquired on the Western Sydney University, Penrith Observatory Telescope. We acknowledge the traditional custodians of the land on which the Observatory stands, the Dharug people, and pay our respects to elders past and present.

BA acknowledges the financial support of the Ministry of Education, Science and Technological

Development of the Republic of Serbia through the contract No. 451-03-68/2022-14/200104.

During work on this paper, G. Djurasevic and J. Petrovic were financially supported by the Ministry of Education and Science of the Republic of Serbia through contract 451-03-9/2021-14/200002.

This research has made use of the SIMBAD database, operated at CDS, Strasbourg, France.

References

- Aigrain, S., Hodgkin, S. T., Irwin, M. J., Lewis, J. R., & Roberts, S. J. 2015, MNRAS, 447, 2880
- Arbutina, B. 2007, MNRAS, 377, 1635
- . 2009, MNRAS, 394, 501
- Awadalla, N. S., & Hanna, M. A. 2005, Journal of Korean Astronomical Society, 38, 43
- Brown, N. J., Waagen, E. O., Scovil, C., *et al.* 2002, *iaucirc*, 7785, 1
- Christopoulou, P.-E., Lalounta, E., Papageorgiou, A., *et al.* 2022, MNRAS, arXiv:2202.12835
- Devarapalli, S. P., Jagirdar, R., Prasad, R. M., *et al.* 2020, MNRAS, 493, 1565
- Drake, A. J., Djorgovski, S. G., Catelan, M., *et al.* 2017, MNRAS, 469, 3688
- Eggleton, P. P. 2012, Journal of Astronomy and Space Sciences, 29, 145
- Gazeas, K. D., Loukaidou, G. A., Niarchos, P. G., *et al.* 2021, MNRAS, 502, 2879
- Handberg, R., Lund, M. N., White, T. R., *et al.* 2021, AJ, 162, 170
- Huang, C. X., Vanderburg, A., Pál, A., *et al.* 2020, Research Notes of the American Astronomical Society, 4, 204
- Jayasinghe, T., Stanek, K. Z., Kochanek, C. S., *et al.* 2020, MNRAS, 491, 13
- Kandulapati, S., Devarapalli, S. P., & Pasagada, V. R. 2015, MNRAS, 446, 510
- Kjurkchieva, D. P., Popov, V. A., & Petrov, N. I. 2018, Research in Astronomy and Astrophysics, 18, 129
- . 2020, New Astronomy, 77, 101352

Abbreviation	RA/DEC	Name
A0006	00 06 50 -35 37 29	ASASSN-V J000649.98-353729.1
LM Psc	00 34 13 20 52 25	ASASSN-V J003412.63+205225.4
A0346	03 46 33.6 41 08 15.8	ASASSN-V J034633.63+410815.8
A0458	04 58 14 06 43 09	ASASSN-V J045813.80+064309.1
A0514	05 14 59 -73 56 15	ASASSN-V J051459.38-735615.4
NSVS 470	07 19 25 41 57 04	ASASSN-V J071924.64+415705.4
V644 Pup	07 27 29 -50 56 30	ASASSN-V J072728.92-505631.1
A0842	08 42 20 -03 03 25	ASASSN-V J084219.98-030325.3
A1037	10 37 37 -37 09 30	ASASSN-V J103736.72-370928.0
A1214	12 14 30.5 -02 57 04	ASASSN-V J121430.46-025704.6
A1249	12 49 08 -29 44 38	ASASSN-V J124907.83-294437.7
A1251	12 51 19 -28 08 25	ASASSN-V J125119.31-280824.8
SSS1315	13 15 59.6 -37 00 17.7	ASASSN-V J131559.62-370018.8
A1407	14 07 13 -30 24 44	ASASSN-V J140712.93-302443.8
A1446	14 46 21 -30 04 40	ASASSN-V J144620.72-300440.9
A1517	15 17 02 14 10 23	ASASSN-V J151701.56+141023.3
A1531	15 31 18 -17 42 36	ASASSN-V J153118.10-174236.0
V396 Lup	16 03 02 -37 49 21.2	ASASSN-V J160302.12-374921.2
A1629	16 29 19.9 35 40 03	ASASSN-V J162919.96+354003.5
A1651	16 51 39.4 22 55 44	ASASSN-V J165139.40+225543.0
V565Dra	17 38 49.82 +57 12 23.2	ASASSN-V J173849.79+571222.6
A1751	17 51 10 03 13 20	ASASSN-V J175109.86+031319.5
A1846	18 46 43.4 -27 36 29	ASASSN-V J184643.38-273629.3
A1847	18 47 37 21 56 06	ASASSN-V J184737.28+215606.0
A1907	19 07 28.30 -53 47 24.7	ASASSN-V J190728.21-534724.9
A1928	19 28 49 -40 45 54	ASASSN-V J192848.87-404554.0
A1946	19 46 45 -04 03 39	ASASSN-V J194644.82-040339.6
A2001	20 01 26 07 37 40	ASASSN-V J200125.92+073739.9
A2003	20 03 04 -02 56 02	ASASSN-V J200303.64-025603.3
A2044	20 44 00 57 52 17	ASASSN-V J204400.26+575216.7
A2044	20 44 52 06 22 31	ASASSN-V J204452.22+062231.3
NSVS 114	20 45 26 16 59 13	ASASSN-V J204525.65+165912.7
A2048	20 48 35 -46 09 42	ASASSN-V J204835.36-460942.4
A2132	21 32 19.4 -53 51 33	ASASSN-V J213219.30-535132.7
A2145	21 45 37 -58 35 00	ASASSN-V J214537.35-583459.9
SSS 2213	22 13 27.3 -44 54 00.5	ASASSN-V J221327.33-445400.3
A2222	22 22 17 37 37 41	ASASSN-V J222217.40+373740.6
A2243	22 43 19 -73 51 18	ASASSN-V J224318.80-735718.0
A2250	22 50 00 -23 16 24	ASASSN-V J224959.89-231623.1
A2258-26	22 58 26 -26 03 36	ASASSN-V J225825.91-260337.8
A2258	22 58 50 13 49 18	ASASSN-V J225849.67+134917.7
NSVS 902	23 19 49 36 03 51	ASASSN-V J231948.59+360350.6
A2348	23 48 23 -40 54 41	ASASSN-V J234823.30-405440.6
V1222 Tau	03 28 26 09 04 24	V1222 Tau
NSVS 431	04 59 45 49 25 03	NSVS 4316778
A0822	08 22 43 19 26 58	ASASSN-V J082243.00+192658.5
GSC 03415-02229	08 27 01 46 28 50	GSC 03415-02229
A0832	08 32 41 23 32 26	ASASSN-V J083240.96+233225.9
NSVS 780	09 06 43 70 03 29	NSVS 780649
PZ UMA	09 29 07 49 51 23	PZ UMA
NSVS 256	10 10 42.7 67 39 31	NSVS 2569022
SX Crv	12 40 15 -18 48 01	SX Crv
A1328	13 28 29 55 52 45	ASASSN-V J132829.15+555245.4
ZZ PsA	21 50 35.2 -27 48 35.5	ZZ PsA

Table 5. Abbreviation, coordinates and ASAS-SN designation of low mass contact binary systems with mass ratios suggesting orbital instability.

- Kobulnicky, H. A., Molnar, L. A., Cook, E. M., & Henderson, L. E. 2022, arXiv e-prints, arXiv:2202.01187
- Kochanek, C. S., Adams, S. M., & Belczynski, K. 2014, *MNRAS*, 443, 1319
- Latković, O., Čeki, A., & Lazarević, S. 2021, *ApJs*, 254, 10
- Li, K., Xia, Q.-Q., Kim, C.-H., *et al.* 2021, *ApJ*, 922, 122
- Liu, L., Qian, S.-B., Soonthornthum, B., *et al.* 2015, *PASJ*, 67, 74
- Lucy, L. B. 1967, *ZAp*, 65, 89
- Martini, P., Wagner, R. M., Tomaney, A., *et al.* 1999, *AJ*, 118, 1034
- Nelson, R. H. 2021, *New Astron*, 86, 101565
- Nelson, R. H., & Robb, R. M. 2015, *Information Bulletin on Variable Stars*, 6134, 1
- Pastorello, A., Mason, E., Taubenberger, S., *et al.* 2019, *AAP*, 630, A75
- Pecaut, M. J., & Mamajek, E. E. 2013, *ApJS*, 208, 9
- Pojmanski, G. 2002, *Acta Astronomica*, 52, 397
- Pollacco, D. L., Skillen, I., Collier Cameron, A., *et al.* 2006, *PASP*, 118, 1407
- Popov, V., Acerbi, F., & Barani, C. 2021, *Research in Astronomy and Astrophysics*, 21, 225
- Rasio, F. A. 1995, *ApJl*, 444, L41
- Ricker, G. R., Winn, J. N., Vanderspek, R., *et al.* 2015, *Journal of Astronomical Telescopes, Instruments, and Systems*, 1, 014003
- Robertson, J. A., & Eggleton, P. P. 1977, *MNRAS*, 179, 359
- Rucinski, S. 1969, *Postepy Astronomii Krakow*, 17, 163
- Rucinski, S. M. 1993, *PASP*, 105, 1433
- . 2001, *AJ*, 122, 1007
- Shappee, B. J., Prieto, J. L., Grupe, D., *et al.* 2014, *ApJ*, 788, 48
- Soker, N., & Tylenda, R. 2003, *ApJl*, 582, L105
- Sriram, K., Malu, S., Choi, C. S., & Vivekananda Rao, P. 2016, *AJ*, 151, 69
- Stępień, K. 2011, *AAP*, 531, A18
- Sun, W., Chen, X., Deng, L., & de Grijs, R. 2020, *ApJS*, 247, 50
- Terrell, D., & Wilson, R. E. 2005, *Ap&SS*, 296, 221
- Tylenda, R., Hajduk, M., Kamiński, T., *et al.* 2011, *A&A*, 528, A114
- Tylenda, R., Kamiński, T., Udalski, A., *et al.* 2013, *AAP*, 555, A16
- Van Cleve, J. E., Caldwell, D. A., Jenkins, J. M., *et al.* 2010, in *American Astronomical Society Meeting Abstracts*, Vol. 215, American Astronomical Society Meeting Abstracts #215, 420.02
- van Hamme, W. 1993, *AJ*, 106, 2096
- Wadhwa, S. S., De Horta, A., Filipović, M. D., *et al.* 2021, *MNRAS*, 501, 229
- Wadhwa, S. S., De Horta, A. Y., Filipovic, M. D., & Tohill, N. F. H. 2022, arXiv e-prints, arXiv:2202.09120
- Yildiz, M., & Doğan, T. 2013, *MNRAS*, 430, 2029
- Zhou, X., & Soonthornthum, B. 2019, *PASJ*, 71, 39
- Zola, S., Rucinski, S. M., Baran, A., *et al.* 2004, *AcA*, 54, 299